On climatological mass, heat, and salt transports through the Barents Sea and Fram Strait from a pan-Arctic coupled ice-ocean model simulation

Wieslaw Maslowski,[1] Douglas Marble,[2] Waldemar Walczowski,[3] Ursula Schauer,[4] Jaclyn L. Clement,[1] and Albert J. Semtner[1]

Received 27 June 2001; revised 1 December 2003; accepted 11 January 2004; published 20 March 2004.

[1] The northward flow of Atlantic Water via the Barents Sea and Fram Strait is modeled, and climatological volume, heat, and salt fluxes into the Arctic Ocean are investigated. We argue that understanding of climate change in the region requires the knowledge of the mean circulation before its variability can be determined. Since estimates of long-term mean fluxes in the region are not available from observations, we present a modeling approach to quantify the climatological circulation and northward transports from the Norwegian Sea into the Arctic Ocean. A coupled ice-ocean model of the pan-Arctic region is configured at a 1/12° and 45-level grid and is integrated for 7 decades using a combination of daily-averaged 1979–2001 European Centre for Medium-Range Weather Forecasts data. Simulated water mass characteristics are compared with climatological atlas and selected observational data. The separation of the Norwegian Atlantic Current into Barents Sea and Fram Strait branches and their relative contributions to the total mass and property input into the Arctic Ocean are quantified. We emphasize the Barents Sea because fewer direct measurements of transports exist there and because water masses are significantly altered along this path by the seasonal ice melt/formation and the freshwater inputs. Under the given atmospheric forcing the Barents Sea outflow is shown to significantly contribute to the boundary flow continuing along the slopes of the Arctic Ocean. On the basis of model results, we argue that the contribution of the Barents Sea branch of Atlantic Water into the Arctic Ocean is equally, if not more, important than the Fram Strait branch. *INDEX TERMS:* 4207 Oceanography: General: Arctic and Antarctic oceanography; 4255 Oceanography: General: Numerical modeling; 4532 Oceanography: Physical: General circulation; 4283 Oceanography: General: Water masses; 4512 Oceanography: Physical: Currents; *KEYWORDS:* Arctic oceanography, sea ice-ocean modeling, Atlantic Water, mass and property fluxes

Citation: Maslowski, W., D. Marble, W. Walczowski, U. Schauer, J. L. Clement, and A. J. Semtner (2004), On climatological mass, heat, and salt transports through the Barents Sea and Fram Strait from a pan-Arctic coupled ice-ocean model simulation, *J. Geophys. Res.*, *109*, C03032, doi:10.1029/2001JC001039.

1. Introduction

[2] Our understanding of the importance of the water mass transformations that occur in the Barents Sea has continued to evolve since it was first understood that there were two possible paths for Atlantic water to enter the Arctic Ocean [*Nansen*, 1906]. Many processes, such as the overall mass and property budgets of the Barents Sea and the monthly, seasonal, and annual current variability, are still undetermined and the subject of much discussion. A factor contributing to the partial understanding of the Barents Sea is that many of the theories and conclusions are necessarily drawn from summer data, due to harsh wintertime conditions in the region. Efforts are underway, such as the European Union funded program "Variability of Exchanges in the Northern Seas" (VEINS), to obtain much needed long-term time series. Several recent studies [*Harms*, 1997; *Loeng et al.*, 1997; *Ozhigin et al.*, 2000; *Ingvaldsen et al.*, 2002] have used a combination of observations and modeling and some of the few available long-term time series to update long-standing theories on Barents Sea circulation and variability of the Atlantic inflow to the Barents Sea. Our efforts are toward enhancing this understanding using high-resolution model output, averaged for 1979–2001 after a total of 7 decades of integration. Our approach is to first quantify the model mean circulation in the region and water mass and property transports into the Arctic Ocean in order to determine variability of these

[1] Oceanography Department, Naval Postgraduate School, Monterey, California, USA.
[2] Fleet Numerical Meteorology and Oceanography Center, U.S. Navy, Monterey, California, USA.
[3] Institute of Oceanology, Polish Academy of Sciences, Sopot, Poland.
[4] Alfred Wegener Institute Foundation for Polar and Marine Research, Bremerhaven, Germany.

0148-0227/04/2001JC001039$09.00

quantities in subsequent analyses. The 23-year-averaged model output is considered to represent mean or climatological conditions.

[3] The remainder of this section discusses the current knowledge of Barents Sea circulation and transports. Section 2 describes the pan-Arctic ice-ocean model, initialization, and forcing. Sections 3 and 4 discuss model results with regard to general oceanography and mass transports respectively. Section 5 focuses on heat and salt transports, the Fram Strait and Barents Sea branches of Atlantic Water and the evolution of temperature and salinity across the Barents Sea. Section 6 discusses specific model-data validations and relative contributions of the Barents Sea and Fram Strait branches of Atlantic Water inflow to the Arctic Ocean. Section 7 contains summary and conclusions.

[4] The warm, salty northward flowing Norwegian Atlantic Current splits in the vicinity of 70°N, with a portion of the flow entering the Barents Sea through the Barents Sea Opening (BSO) as the North Cape Current, and the remainder continuing north along the Norwegian Sea/Barents Sea shelf break toward Svalbard, becoming the West Spitsbergen Current [*Aagaard*, 1989]. See Figure 1b for a map of the region and locations of key features. For the purposes of this discussion, the two main paths of flow into the Barents Sea from the Norwegian Sea are the Norwegian Coastal Current and the North Cape Current. The Norwegian Coastal Current is the fresher of the two and travels closest to the Norwegian coast. The North Cape Current is defined as that branch entering the Barents Sea primarily via the Bear Island Trough.

[5] The flow through the BSO, as implied by the hydrographic conditions, was thought to be relatively stable with seasonally variable inflow in the southern two thirds and outflow in the northern third [*Blindheim*, 1989; *Pfirman et al.*, 1994]. Results from 1 year of measurements obtained from several moorings across a section from Bear Island to Fugloya, north of Norway, [*Ingvaldsen et al.*, 2002] indicate the predominantly barotropic flow may vary between a broad Atlantic inflow, outflow all the way south to 72°N, or inflow and recirculation in nearby cells. *Ingvaldsen et al.* [2002] did not observe a seasonal signal in the inflow. However, their measurements did indicate current intensification, strong lateral velocity gradients and a distinct surface-intensified relatively high velocity core of inflow caused by the frequent passing of atmospheric lows in the winter. During the summer, the inflow area was seen to be wider and there were two lower-velocity cores of inflow.

[6] During certain periods, the net flow was observed to be from the Barents Sea to the Norwegian Sea [*Ingvaldsen et al.*, 2002]. This reversal of the flow was interpreted to be due primarily to variations in the atmospheric pressure. Some of the high net flow was attributed to the presence of transient mesoscale eddies. The monthly mean volume transport across the section covered by moorings, which did not represent the full section between Bear Island and Fugloya, fluctuated over a range of 11 Sv (1 Sv = 10^6 m^3 s^{-1}) between 5.5 Sv into and out of the Barents Sea [*Ingvaldsen et al.*, 2002].

[7] Another source of water to the Barents Sea is the colder and fresher Norwegian Coastal Current, which carries waters originating from the Baltic Sea and Scandinavian runoff eastward, along the Norwegian and Russian coasts [*Maslowski and Walczowski*, 2002]. Owing to the relatively small river input into the Barents Sea, the Norwegian Coastal Current is considered the main freshwater source, in addition to ice melt, for the region. An updated schematic of the Barents Sea circulation [*Ozhigin et al.*, 2000] shows this current hugging the coast and following the 100 m contour. Further east and north, a portion of the coastal current joins the Bear Island Trough inflow at the southern edge of the Eastern Basin. The Norwegian/Murmansk Coastal Current continues to the east and it is not clear how much of it mixes with White Sea and Pechora River outflow prior to entering the Kara Sea via the Kara Gate. Values between 0.05 and 0.7 Sv [*Loeng et al.*, 1997], up to 1 Sv [*Aagaard and Greisman*, 1975], have been estimated for the flow south of Novaya Zemlya to the Kara Sea.

[8] A percentage of the North Cape Current recirculates within the Bear Island Trough, flowing south, parallel to the cold Bear Island Current, and then exiting the Barents Sea [*Pfirman et al.*, 1994; *Parsons et al.*, 1996]. This recirculation within the Bear Island Trough was seen to be relatively stable at ~1.0 Sv, but with high outflow episodes occurring during winter and early spring [*Ingvaldsen et al.*, 2002]. The remainder of the North Cape Current flows south of the Central Bank, following the bathymetry, to the Eastern Basin. *Ozhigin et al.* [2000] demonstrate that Eastern Basin Deep water is local in origin, formed by significant modification of Atlantic water, rather than Arctic water carried southwest by the Central Current. Their results show no indication of Arctic water transport into the Eastern Basin from the northeast and a dome shaped structure of waters in the Eastern Basin, resulting in well pronounced cyclonic circulation in that area.

[9] The now significantly modified Atlantic water travels N-NE as the Novaya Zemlya Current, staying west of the Novaya Zemlya Bank and exiting the Barents Sea between Frans Josef Land and Novaya Zemlya [*Ozhigin et al.*, 2000], the main outflow region of the Barents Sea. Estimates of average mass transport leaving the Barents Sea are on the order of 2 Sv [*Loeng et al.*, 1993; *Rudels and Friedrich*, 2000], varying between 1 and 3 Sv with a distinct maximum during the cold season and a minimum during summer [*Loeng et al.*, 1997].

[10] The modified Atlantic water then transits the northern Kara Sea where the majority enters the Nansen Basin via the St. Anna Trough [*Rudels*, 1987; *Harms*, 1997] and then moves eastward along the slope, displacing the Fram Strait branch of Atlantic Water (FSBW) away from the slope [*Schauer et al.*, 1997]. During summer, a portion of the Novaya Zemlya Current may continue south along the east coast of Novaya Zemlya [*Harms and Karcher*, 1999]. Using a series of moorings in the Kara Sea, *Johnson et al.* [1997] found no evidence of warm flow from the Barents Sea around the northern end of Novaya Zemlya. The focus of their efforts was further to the south and they do acknowledge the density of their observation network may not have been sufficient to resolve this particular feature.

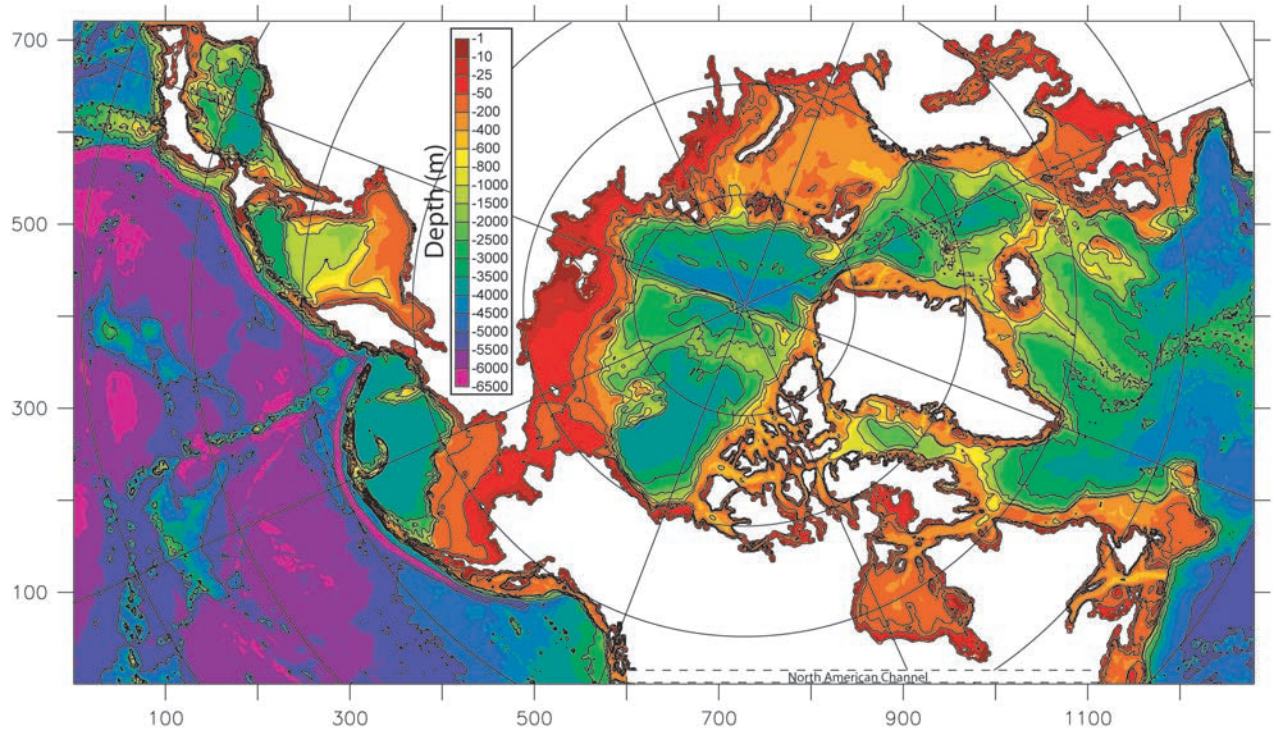

Figure 1a. The model domain and bathymetry. Two dashed lines across Canada indicate the location of an artificial channel connecting the North Atlantic with the North Pacific to balance the net northward water transport through Bering Strait.

[11] A portion of the West Spitsbergen Current recirculates within the Storfjord Trough, while the majority continues north along the shelf break [*Pfirman et al.*, 1994]. West of Svalbard, the West Spitsbergen Current splits, with the Return Atlantic Current heading west and eventually south in the Greenland Sea, while the remainder enters the Arctic Ocean via Fram Strait. This branch entering Fram Strait splits again, one branch travels north along the western edge of the Yermak Plateau and the remainder continues to the east along the northern slope of the Barents Sea [*Rudels et al.*, 1994]. Owing to interaction with the ice encountered in Fram Strait and north of Svalbard, the surface signature of the Atlantic water is obscured as it loses its warm and saline characteristics. The Atlantic core, consisting of water >0°C, becomes an intermediate water mass and is denoted as the Atlantic Layer [*Rudels and Friedrich*, 2000]. Limited amounts of Atlantic Water are thought to enter the Barents Sea from the north via Frans Josef-Victoria Trough as a near-bottom water mass [*Pfirman et al.*, 1994]. *Loeng et al.* [1997] use values obtained from Russian literature of 0.4 Sv entering the Barents Sea from the Arctic Ocean and 0.1 Sv exiting the Barents Sea to the Arctic Ocean between Svalbard and Frans Josef Land. The East Spitsbergen Current and the Persey Current, west of Frans Josef Land, bring cold, fresh Arctic Water from the north into the Barents Sea. The cold, high-velocity Hopen-Bjornoya Current (of order several cm s^{-1}) travels south and west along the eastern edge of the Spitsbergen Bank. Its interaction with the recirculating North Cape Current is marked by the Arctic Polar Front [*Loeng*, 1991; *Pfirman et al.*, 1994; *Parsons et al.*, 1996].

2. Model Description

[12] The coupled ice-ocean model domain (Figure 1a) includes the Sea of Japan, the Sea of Okhotsk, the sub-Arctic North Pacific and North Atlantic Oceans, the Arctic Ocean, the Canadian Arctic Archipelago (CAA) and the Nordic Seas. The domain was chosen to include all major inflow and outflow areas of the Arctic Ocean and all of the Northern Hemisphere seasonally ice-covered seas. The region of interest for this paper (Figure 1b) includes the Barents and Kara Seas, the northern Norwegian Sea, Fram Strait and the southern edge of the Eurasian Basin. This region is far away from the artificially closed lateral boundaries in the North Atlantic, located at 40°–45°N, assuring no effect on analyzed results. Additional details of the approach along the lateral boundaries are discussed throughout this section.

[13] The model is configured on a 1/12°, or ~9 km, rotated spherical coordinate grid. The high horizontal resolution and the large domain allow the simulation of most of the important processes in the Arctic Ocean and realistic exchanges between the Pacific Ocean, the Arctic Ocean, the Canadian Arctic Archipelago, and the North Atlantic. The model is considered eddy permitting as features down to ~36 km (four grid points) can be resolved. With the radius of deformation in the Arctic Ocean <10 km, many of the smaller features will not be well represented. Regional comparisons of eddy kinetic

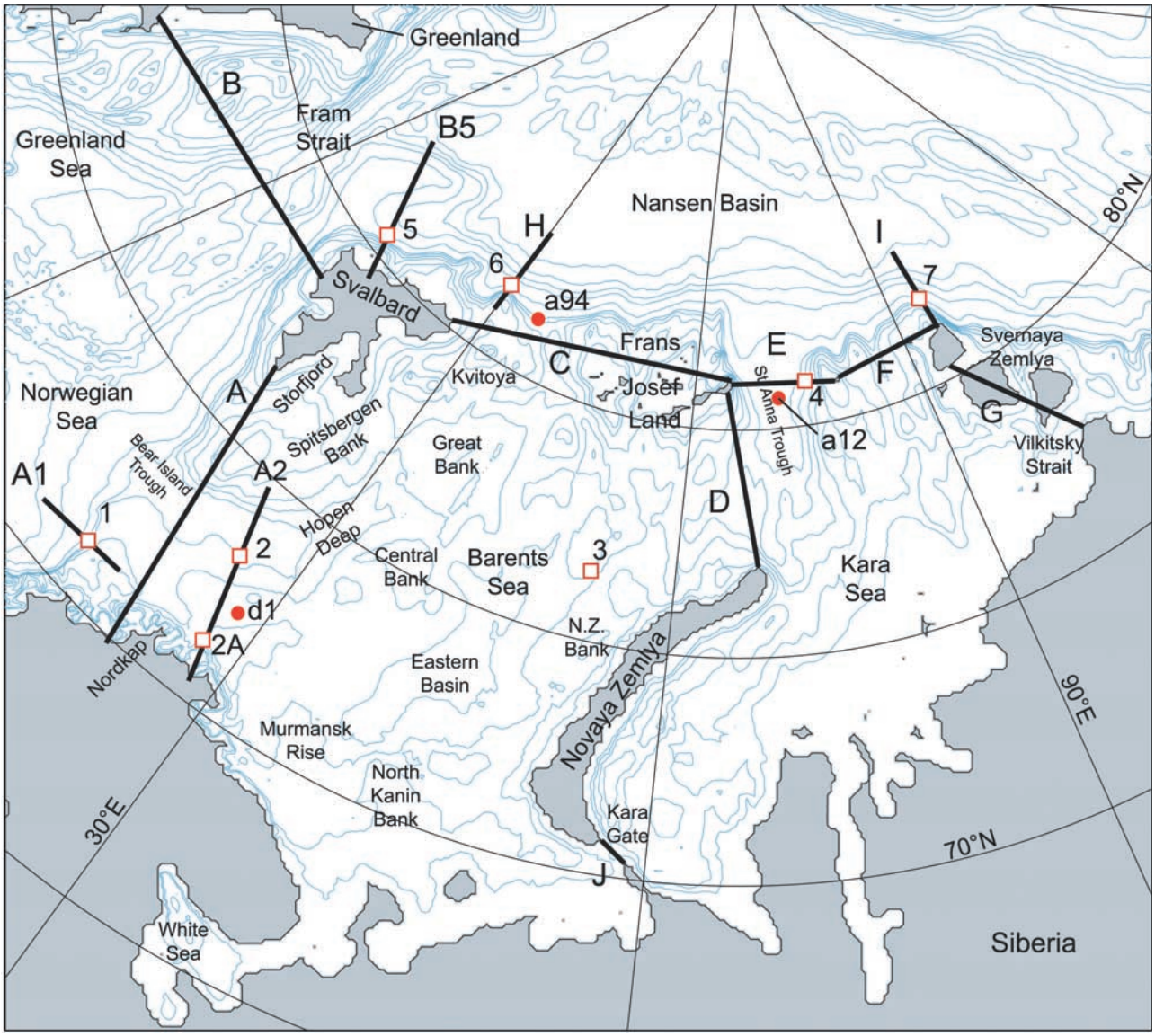

Figure 1b. Barents and Kara Seas bathymetry (m) and location of model sections and stations. Solid lines and letters denote sections. Hollow squares and numbers identify stations. Locations of observational data are indicated by red dots: d1, Dalnye Zelintsi 1 (July 1991); a12, *Polarstern* ARKXII (August/September 1996); a94, *Polarstern* ARKIX_4 (August/September 1993).

energy with a previous 18 km version of the coupled ice-ocean model [*Zhang et al.*, 1999; *Maslowski et al.*, 2000] reveal a fourfold to tenfold increase in eddy kinetic energy in the 9 km model. Vertically, the model is divided into 45 z coordinate levels. The 11 layers in the first 100 m and 19 layers in the first 500 m are chosen to provide accurate representation of the vast Arctic continental shelves and slopes. The complex bathymetry of the deep basins and steep submarine ridges is well represented by 22 200- to 300-m-thick layers from 1000 to 6250 m deep. Setting the maximum depth in the model to 6250 m precludes modeling deep ocean trenches in the Pacific Ocean, but it is felt this will not adversely impact the primary goals of the simulation: modeling sea ice and ocean characteristics and circulation in the Arctic Ocean. Model bathymetry south of 64°N is derived from the National Geophysical Data Center ETOPO5 database. North of 64°N, the bathymetry is based on the 2.5 km resolution International Bathymetric Chart of the Arctic Ocean (IBCAO) [*Jakobsson et al.*, 2000] digital bathymetry data set.

[14] The model lateral boundaries, including those for river runoff, are closed, allowing no mass or momentum transfer across them. In an effort to balance the net flow of Pacific Ocean water into the Arctic Ocean, a U-shaped 500 m deep, 162 km (18 grid point) wide channel was created through North America connecting the Atlantic Ocean to the Pacific Ocean (Figure 1a). Flow through the Bering Strait and the channel is not prescribed. A westward wind forcing of 1.75 dyne cm^{-2} is prescribed along the channel, which results in a net average northward Bering Strait flow varying between 0.5 and 0.8 Sv into the Arctic

Ocean [*McClean et al.*, 2001], close to the observed early 1990s mean flow through the Bering Strait of 0.83 Sv [*Roach et al.*, 1995].

[15] The regional ocean model adapts the Los Alamos National Laboratory (LANL) Parallel Ocean Program (POP) model [*Dukowicz and Smith*, 1994] with an added free surface [*Killworth et al.*, 1991; *Semtner*, 1995], which evolved from the *Semtner and Chervin* [1992] global ocean model. The free surface, combined with high resolution allows the use of unsmoothed, very realistic bathymetry. Owing to computational constraints, many earlier ocean models were formulated using a rigid lid assumption. To avoid numerical instability in rigid lid models, it was necessary to smooth the bathymetry to eliminate excessively steep depth gradients, which had the potential to over-accelerate flow along the bottom [*Killworth et al.*, 1991; *Dukowicz and Smith*, 1994].

[16] In the model, we assume hydrostatic balance and make the Bousinessq approximation. The finite difference scheme integrates the primitive equations in spherical coordinates on an Arakawa B grid [*Mesinger and Arakawa*, 1976]. To satisfy numerical stability criteria, the ocean time step is 480 s (8 min). To eliminate the convergence of meridians at the North Pole inherent in spherical coordinates, the model grid was rotated, placing the model equator along the meridians 26°W and 154°E. The sea ice model uses viscous plastic ice rheology [*Zhang et al.*, 1999] and the zero-layer approximation for heat conduction through ice [*Semtner*, 1976]. The surface heat budget follows *Parkinson and Washington* [1979]. The ice model time step is 48 min.

[17] The ocean was started from rest and initialized using three-dimensional temperature and salinity fields from the University of Washington Polar Science Center Hydrographic Climatology 1.0 (PHC) [*Steele et al.*, 2000] interpolated onto the model grid. The PHC is a combination of the 1998 version of the World Ocean Atlas [*Antonov et al.*, 1998; *Boyer et al.*, 1998] with the regional Arctic Ocean Atlas [*Environmental Working Group*, 1997, 1998]. The ice model was initialized with a uniform 2-m-thick layer of ice over water with temperature <0.0°C in the beginning of January. This method was chosen to avoid the shock to the surface freshwater budgets of the North Atlantic and North Pacific Oceans, which would result from melting a slab of ice in regions where sea ice is not normally present.

[18] During the first 27 years of spin-up, the model is being forced with a 15-year mean, annual cycle of daily averaged atmospheric forcing derived from the European Center for Medium Range Weather Forecasting 1979–1993 reanalyzed data. During the second decade of spin-up, deep acceleration was turned on. This is a numerical method used to save computational time, which increases the time step applied to temperature and salinity diffusion calculations at depth, where water mass properties change at a much slower rate. The time step in the top 16 layers (0–220 m) remains 8 min. Below 220 m, the time step applied to the temperature and salinity diffusion equations increases smoothly by a factor from 1 to 10, through level 33 (3050 m). Below 3050 m in the model, the deep ocean evolves 10 times faster than the upper 220 m. Using this method, at the end of 10 years of model integration, the deep ocean has been effectively integrated for 100 years. Deep acceleration was turned off during the remaining 7 years of the initial spin-up, which was then followed by a 6-year run forced with the repeated 1979 daily averaged European Centre for Medium-Range Weather Forecasts (ECMWF) reanalyzed data. During that time and the subsequent 15-year integration with the repeated 1979–1981 daily averaged ECMWF data the model was forced toward conditions of the late 1970/early 1980, in order to begin the 1979–2001 interannual simulation. Beginning in year 42 of spin-up, river runoff forcing was prescribed through restoring to temperature and salinity as a function of daily-averaged annual cycle of each river discharge, including Russian (Dvina, Pechora, Ob, Yenisey, Kotuy, Lena, Indigirka, and Kolyma), Mackenzie, and Yukon rivers.

[19] Atmospheric forcing fields include 10 m east-west and north-south (u and v) wind velocity components, surface pressure, temperature and dew point, and long-wave and short wave radiation. The forcing data, as described earlier, were interpolated onto the model grid. The ocean surface level, 5 m thick, is restored on a monthly timescale to monthly PHC temperature and salinity climatology, as a correction term to the explicitly calculated fluxes between the ocean and overlying atmosphere or sea ice. Additional discussion of the surface restoring in models of the Arctic Ocean can be found in the work of *Steele et al.* [2001]. A 4° wide, or 48-grid-point-thick, curtain along the model domain boundary ocean points is restored on a 10 day timescale to annual average PHC temperature and salinity climatology. The curtain restoring at the model boundaries partially compensates for the effects of the domain boundaries in the vicinity of strong midlatitude currents. The boundaries are far enough away from the primary region of interest so the impact of the curtain restoring is minimal.

[20] In considering ocean climatology and atmospheric forcing bias, the time span of the merged ocean climatology data sets [*Steele et al.*, 2000, Table 1] shows the 1946–1994 data were collected during periods of anticyclonic and cyclonic atmospheric forcing regimes [*Proshutinsky and Johnson*, 1997; *Johnson et al.*, 1999]. Thus it is felt there is no strong ocean climatology bias toward either regime. The combination of the Environmental Working Group Arctic Ocean Atlas with the World Ocean Atlas (WOA) has helped remove much of the strong summer bias in the WOA Arctic Ocean climatology. The atmospheric forcing is an average from time periods dominated by both anticyclonic and cyclonic regimes. A comparison of the mean 0–50 m Arctic Ocean circulation with representative ocean surface circulation patterns for each regime [*Proshutinsky and Johnson*, 1997; *Maslowski et al.*, 2000, 2001] shows a flow in between the two extremes, with a medium sized Beaufort Gyre and a Transpolar Drift Stream aligned along the Mendeleyev Ridge. The model results used in this analysis consist of 276 monthly averaged ocean data sets from the 1979–2001 run, 365 daily ocean data sets from year 1987 and 365 daily ice data sets from year 1987.

3. Model Physical Oceanography

[21] Since we analyze 23-year averaged model output, we are not expecting to recreate specific conditions related to

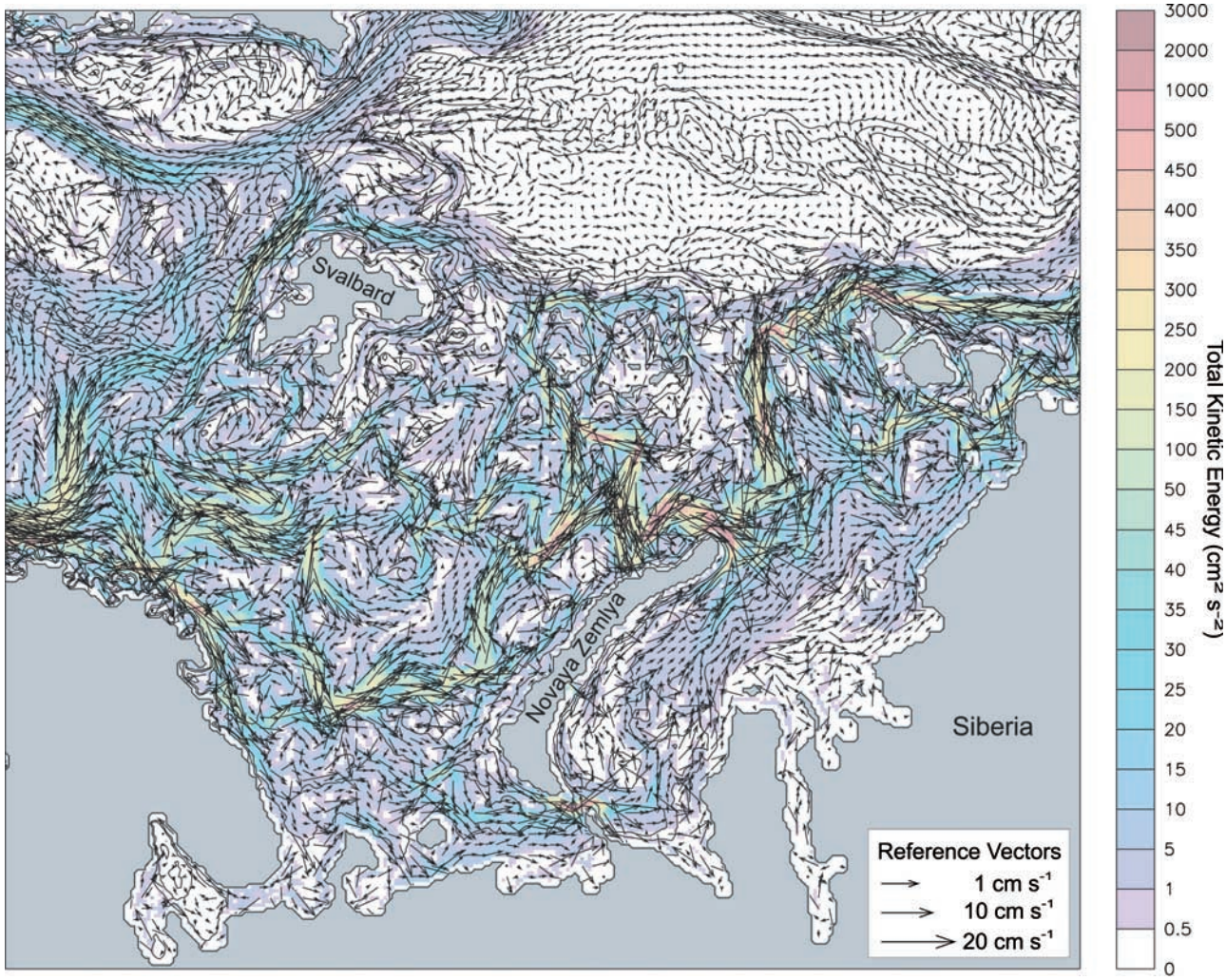

Figure 2. Twenty-three-year mean (1979–2001) depth-averaged 0–223 m (model levels 1–16) velocity (cm s^{-1}). Every third vector is shown. Color shading represents total kinetic energy (cm^2 s^{-2}) at every grid point.

specific dates. Nevertheless, model mean results show climatological features, such as the summer freshening of surface waters in the Barents Sea, and important processes, such as mass and property transports and water mass transformations, which are known to occur in the Arctic Ocean and its adjacent seas, at the highest resolution to date for a large-domain coupled ice-ocean model.

[22] The 23-year average velocity in the top 16 levels (0–223 m) in the Barents Sea (Figure 2) is predominantly west to northeast and constrained by bathymetry. It shows a broad, meandering Norwegian Atlantic Current in the northern Norwegian Sea, a strong, narrow Norwegian Coastal Current and Atlantic Water inflow and recirculation in Bear Island Trough. The Norwegian Atlantic Current is represented as a broad (100–130 km) flow with an annual mean salinity above 35.15 psu, temperature of 5°–6°C and velocity of 4–5 cm s^{-1} (Figures 3a, 3c, and 3e) averaged over the 300-m-thick core.

[23] The North Cape Current flows into the Bear Island Trough along its southern edge and a percentage turns north and then recirculates along the 400 m isobath back out to the Norwegian Sea and the West Spitsbergen Current, another percentage follows the 300 m contour clockwise around the Hopen Deep. The majority of the North Cape Current continues east along the southern flank of Central Bank (Figure 2) into the Eastern Basin. In model section A2, from the Norwegian Coast east of Nordkap toward Bear Island (Figures 1b, 3b, 3d, and 3f), the Norwegian Coastal Current is narrower (~50 km versus ~130 km based on the velocity distribution), colder (4.5°C versus 5.5°C), fresher (34.2 psu versus 35.10 psu), and faster (5–6 cm s^{-1} versus 2–3 cm s^{-1}) than the North Cape Current in Bear Island Trough. There are bands of recirculation in between the North Cape Current and the Norwegian Coastal Current and bands of inflow and outflow, along the southern flank of Spitsbergen Bank. In monthly averaged sections across Bear Island Trough (not shown) the inflow in wintertime is narrower and stronger, with a maximum in January, and it is weakest in summer, features similar to those reported by *Ingvaldsen et al.* [2002]. In general, the model distribution of temperature, salinity and velocity in Bear Island Trough is similar to

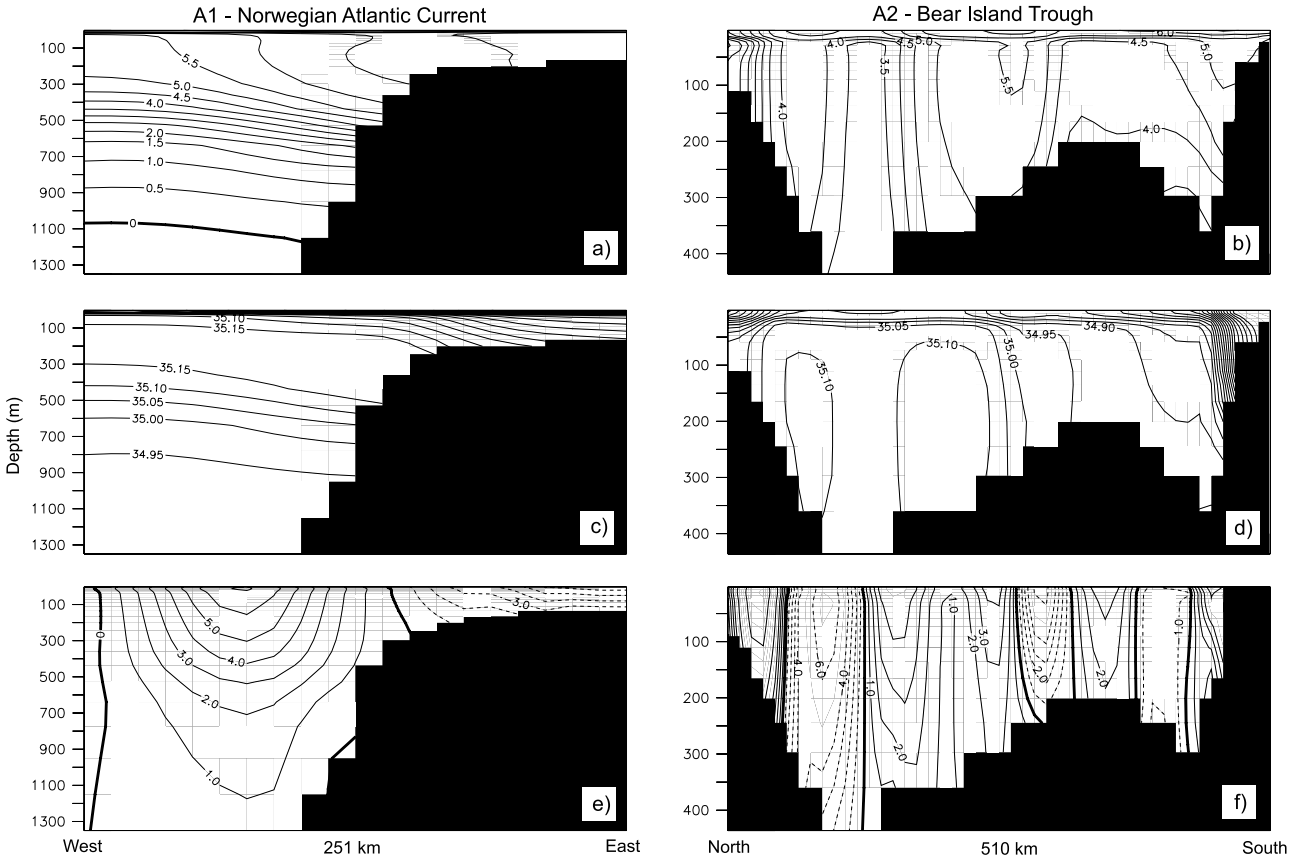

Figure 3. Vertical distribution of annual (a–b) average potential temperature (°C), (c–d) salinity (psu), and (e–f) velocity (cm s^{-1}) across the Norwegian Atlantic Current (model section A1, left) and the Bear Island Trough (model section A2, right). Note the differing vertical and horizontal scales. Positive velocity contours represent northward and eastward flows.

the observed distribution [*Loeng et al.*, 1997] with outflow constrained to the northern one third (Figure 3f).

[24] In the northwestern corner of the region, the cold, narrow East Spitsbergen Current entering the Barents Sea between Svalbard and Kvitoya, is well represented in the 23-year average velocity field. The Persey Current is a broad southward flow between Svalbard and Frans Josef Land and across the Great Bank. The Hopen-Bjornoya Current travels along the southern flank of Spitsbergen Bank. The polar front associated with it is readily visible in the winter and summer 0–50 m ocean temperature and salinity fields (Figures 4a–4d). The general path of the warm, salty Atlantic Water, entering the Barents Sea via Bear Island Trough, traveling east, south of the Central Bank, and then N-NE along the west side of Novaya Zemlya Bank, rounding the northern tip and exiting the Kara Sea via St. Anna Trough, can also be seen in the seasonal temperature and salinity fields. Several quasi-permanent cyclonic eddies can be identified in the south-eastern Barents Sea, associated with distinct bathymetric features like the Nordkap, the Central Bank, Murmansk Rise, North Kanin Bank, and the southern end of the Eastern Basin (Figure 2).

[25] On both sides of the Eastern Basin, the mean deep flow is northward, with the main branch of warm Atlantic water following the eastern side, toward Novaya Zemlya Bank. A cyclonic circulation in the Eastern Basin is not readily visible in the 23-year average velocity field. However, during the winter season there is a distinct cyclonic circulation around the Eastern Basin, and intensification of currents in general. In agreement with *Ozhigin et al.* [2000], model results show no evidence of Arctic Water transport into the Eastern Basin from the northeast. The predominantly barotropic, northward flows of Atlantic Water on either side of the Eastern Basin merge at the northern end, isolating the Eastern Basin from advection of Arctic water from the north.

[26] Prior to exiting the Barents Sea, the Novaya Zemlya Current splits, with one part traveling north, toward the southern coast of Frans Josef Land. A portion of the northward flow exits the Barents Sea via the Frans Josef–Victoria Trough, west of Frans Josef Land. Atlantic Water exiting the Barents Sea via the eastern edge of this trough is readily visible in animations of 100–200 m and 200–300 m monthly average temperature and salinity. Atlantic origin water, which has entered the Arctic Ocean via Fram Strait, enters the Barents Sea via the western side of the Frans Josef-Victoria Trough. Both of these exchanges occur primarily during the summer. The majority of the modified Atlantic Water flow headed toward Frans Josef land turns east and then back to the south, guided by bathymetry, to meet the remainder of the

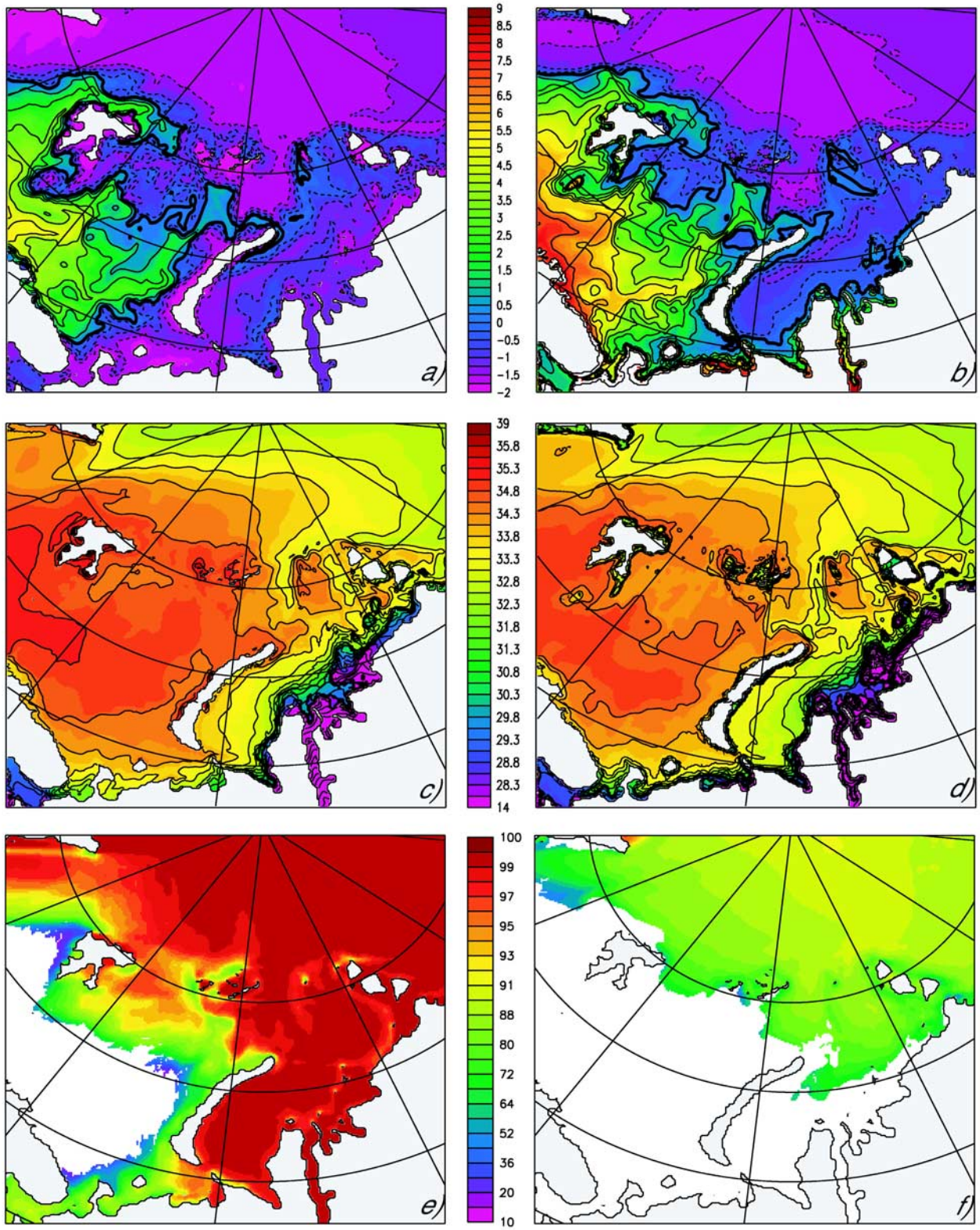

Figure 4. Distribution of temperature and salinity in the upper 0–53 m (model levels 1–8) and sea ice concentration for various seasons. Winter 23-year mean (January/February/March) (a) potential temperature (°C) and (c) salinity (psu). Summer 23-year mean (July/August/September) (b) potential temperature (°C) and (d) salinity (psu). (e) Winter 23-year mean (January/February/March) sea ice concentration (%). (f) Summer 23-year mean (July/August/September) sea ice concentration (%).

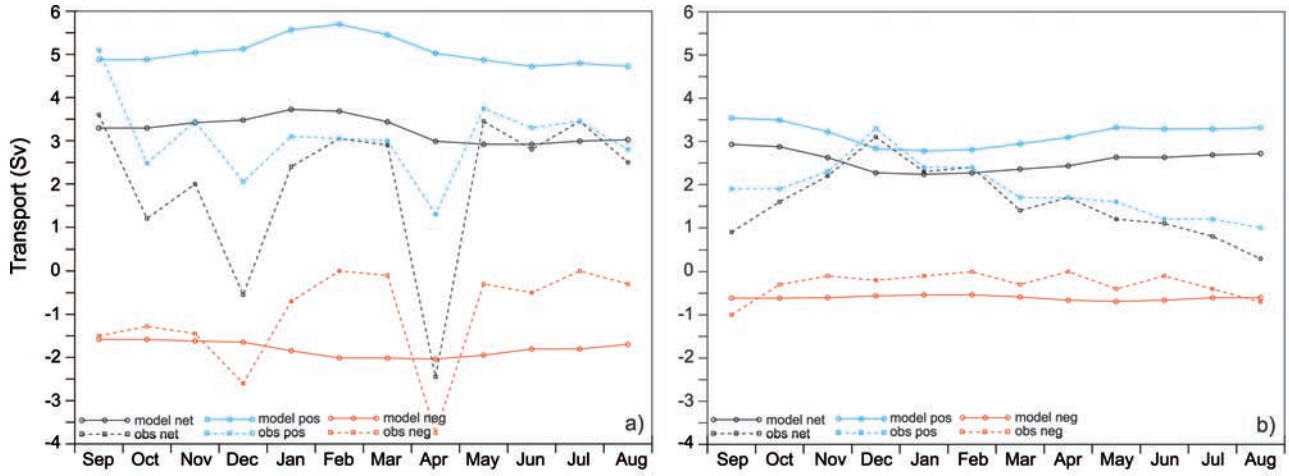

Figure 5. Twenty-three-year monthly mean volume transport (Sv), from the model and from observations, (a) through the strait between Svalbard and Norway and (b) through the strait between Frans Josef Land and Novaya Zemlya. Observational data were taken from *Ingvaldsen et al.* [2000] for Figure 5a and from *Loeng et al.* [1997] for Figure 5b.

northeastward flowing Novaya Zemlya Current, west of the northern tip of Novaya Zemlya.

[27] The Novaya Zemlya Current in the vicinity of station 3 (Figure 1b) has an annual average core velocity of $\sim$30 cm s^{-1}, a salinity of 34.99 psu and a temperature of 3.8°C. The Novaya Zemlya Current finds a narrow, 200–220 m deep gap in the sill between Frans Josef Land and Novaya Zemlya [*Jakobsson et al.*, 2000] and enters the southern reaches of the Santa Anna Trough. Here the majority of the flow follows the bathymetry between the 200 and 300 m contours and travels toward the Nansen Basin along the eastern edge of Santa Anna Trough. The flow then travels east along the shelf break, with some water recirculating through Voronin Trough.

[28] A portion of the Novaya Zemlya Current continues south around the eastern tip of Novaya Zemlya into the Kara Sea. Both branches of the warm flow are reflected in the summer and winter average ice cover (Figures 4e and 4f), as a decrease in concentration along their path. The thermodynamically driven thinning of the ice cover along the path of the warm flow is clearly visible in animations of daily ice concentration and thickness. This thermodynamic effect is strong enough to be distinguished from the wind driven flow of ice in the northern Kara Sea, even in midwinter.

[29] Comparison of matching 0 m, 30 m, 50 m, 100 m and 200 m monthly average temperature and salinity fields (not shown) with the 1998 National Oceanic and Atmospheric Administration Barents Sea Climatic Atlas [*Matishov et al.*, 1998] reveal the North Cape Current in the model Barents Sea being comparable to climatology. There is a significant improvement compared to the same oceanic and sea ice fields from the model spin-up with the climatological forcing. This is possibly a combined effect of more realistic atmospheric forcing and the inclusion of annual cycle of river runoff in the 1979–2001 simulation.

[30] The location of the Barents Sea Polar Front (BSPF), the seasonal summer northward pulse of warmer water and the summer freshening along the Russian coast in the model agree well with the climatology. In September, the BSPF is not readily discernible in the surface temperature field. Otherwise, throughout the year, it is well defined by the 2°–4°C isotherms and the 34.6–34.9 psu isopleths. As in the climatology, the seasonal signal in temperature and salinity variability decreases with depth. In the summer at 200 m depth, the small northward pulse in warmer and saltier water reaches just north of the Eastern Basin. The summer northward pulse of warmer water at the surface can be seen entering the St. Anna Trough, in comparison with the limited northern extent of the summer warm water pulse in deeper water.

4. Mass Transports

[31] Mass, heat and salt transports were calculated at the boundaries of the Barents Sea and at Fram Strait. Ice-ocean freshwater fluxes are not addressed directly in this paper. However, the influence of ice growth and melt can be seen in changes in the seasonal distribution of 0–50 m temperature and salinity (Figure 4). The alignment of each section in Figure 1b was chosen to ensure positive values of volume transport into the Arctic Ocean. For north-south-aligned sections (sections A, A2, B5, D, H and I in Figure 1b) positive values of volume transport indicate transport to the east or along the path of Atlantic Water inflow to the Arctic Ocean.

[32] An annual average volume transport of 5.07 Sv enters the Barents Sea between Norway and Svalbard, and $\sim$1.8 Sv exits through the same section, yielding a net annual average transport of 3.27 Sv (Table 2). The magnitudes of the transports are somewhat larger than those obtained from observations [*Loeng et al.*, 1997; *Ingvaldsen et al.*, 2002]. One of the reasons for that might be the absence of tides in this model, which we have seen in test experiments with M2 semidiurnal tide [*Parsons*, 1995] to produce tidal residual currents opposite to the mean flow up to 5 cm s^{-1}. Another cause for the difference may lie in the method of calculation. For

the model results, transport is calculated across the entire section, coastline to coastline, whereas the boundaries of transports calculated from observations are determined by the mooring locations and exclude flow shoreward of the moorings. A comparison of model monthly-averaged volume transport through the Svalbard-Norway section with values from a yearlong time series obtained by current meter moorings between Bear Island and Fugloya [*Ingvaldsen et al.*, 2002] (Figure 5a) shows considerably less variability in the model output, no clear seasonal signal and no indication of periods of net outflow, which suggest some problems with the atmospheric forcing, possibly underrepresentation of eddy field, and will require further investigation including nonaveraged model output for years comparable to observations.

[33] Between Svalbard and Frans Josef Land, a net 0.36 Sv enters the Barents Sea from the Arctic Ocean. From reviewing animations of the monthly mean vertical distribution of temperature, salinity and velocity across this section, the flow into the Barents Sea (1.17 Sv) is a mix of Polar surface water and warm Fram Strait Branch Atlantic water. The outflow to the Arctic Ocean (0.81 Sv) is cold, Barents Sea-modified Atlantic water. There is a weak seasonal signal in the transport, with an increase in both inflow and outflow in the winter. The net Svalbard-Norway and Svalbard-Frans Josef Land inflows are balanced by net outflow between Frans Josef Land and Novaya Zemlya and flow through the Kara Gate, within a ~1% margin of error.

[34] The outflow between Frans Josef Land and Novaya Zemlya is concentrated in an ~90 km wide band in the southern one quarter of the section, and it reaches speeds of up to 30 cm s^{-1} in the wintertime. Comparing the model transport between Frans Josef Land and Novaya Zemlya (Figure 5b) with that obtained from 1 year of current meter measurements [*Loeng et al.*, 1997], the mean magnitudes of the transports agree, yet the observed seasonal signal, especially in the eastern (positive) component of the flow is not visible in model results. This may again be attributed to the insufficient model resolution to account for smaller eddies and to dampening of the seasonal cycle in average model output. South of Novaya Zemlya, the predominantly eastward flow through Kara Gate has a winter maximum of 0.45 Sv and a summer minimum of 0.2 Sv, and a net annual average transport from the Barents Sea to the Kara Sea of 0.32 Sv. The only periods of weak westward flow through Kara Gate, ~0.01 Sv, are August and September. The majority of the Barents and Kara Seas outflow occurs via the St. Anna Trough, ~2.92 Sv versus ~0.72 Sv via Voronin Trough and 0.32 Sv via Vilkitsky Strait.

5. Heat and Salt Transports

[35] To compare the flow into the Arctic Ocean via Fram Strait with that through the Barents Sea, mass, heat and salt transports were calculated through Fram Strait and along the northern Barents Sea shelf slope (Table 2, sections *B, H* and *I*, Qheat is referenced to −0.1°C and Qsalt is referenced to 0.0 psu).

[36] The amount of heat flowing into the Barents Sea, between Svalbard and Norway, is more than twice that of the amount of heat entering the Arctic Ocean via Fram Strait (i.e., 106 TW compared to 47 TW). However, the Barents Sea branch loses almost all its heat prior to exiting the Barents Sea. The net amount of heat entering the Barents Sea between Svalbard and Norway, 78 TW, is toward the high end of estimates from observations [*Simonsen and Haugan*, 1996]. The mean heat loss from the Barents Sea is about 77 TW. This estimate is in the upper range of the published heat loss between 28 and 80 TW [*Simonsen and Haugan*, 1996] and it is in the lower range of 42−162 TW, estimated by *Simonsen and Haugan* [1996] derived using different parameterizations of the sea surface heat budget. In the model, net 1.3 TW enters the Arctic Ocean via the St. Anna Trough. This is ~12% of the heat transported via the Fram Strait branch of Atlantic Water across section H, east of the Yermak Plateau along the 30°E and about 800 km upstream of the St. Anna Trough. A small heat flux of 0.28 TW enters the Barents Sea via the Voronin Trough.

[37] The amount of net heat entering the Arctic Ocean from the Barents Sea, via St. Anna Trough is roughly 15% of the net heat transport across section I, north of Severnaya Zemlya (~8.6 TW). Hence under the atmospheric forcing conditions during 1979−2001, the Fram Strait branch of Atlantic Water accounts for ~85% of heat transported in the boundary current along the shelf slope, north of Severnaya Zemlya.

[38] The salt transport into the Barents Sea (across section A) and through Fram Strait are of similar magnitude, $\sim 177 \times 10^3$ kg s^{-1} compared to 223×10^3 kg s^{-1}, respectively. The salt export from the Barents Sea into the Arctic Ocean via St. Anna and Voronin troughs is $\sim 126 \times 10^3$ kg s^{-1}, indicating that the contributions due to ice melt/formation and freshwater inflow account for roughly 30% freshening within the Barents Sea. The salt export through the two troughs is over 50% larger than that of eastward salt transport of the Fram Strait branch (83×10^3 kg s^{-1}) across section H, east of Yermak Plateau. It constitutes over 60% of the total of 203×10^3 kg s^{-1} salt transport across section I, north of Severnaya Zemlya. Since salt content determines density in the polar regions and because of the closer proximity of St. Anna and Voronin trough sections (compared to section H) to Severnaya Zemlya we argue that the Barents Sea branch plays a dominant role in setting the salt and density content of the circum-Arctic boundary current.

6. Discussion

[39] A comparison of the mean net volume transports via the two pathways helps to further evaluate the relative importance of each branch on the central Arctic Ocean circulation and water mass properties. The mean net volume transport through the Svalbard-Norway section is 3.27 Sv (std = 0.58 Sv), with 5.07 Sv (0.71 Sv) entering the Barents Sea and 1.8 Sv (0.46 Sv) recirculating back to the Greenland Sea. The numbers in parentheses above and in the rest of the discussion denote standard deviations calculated from the 23-year monthly mean time series and are also shown in Table 2. The respective transports through Fram Strait (from the surface to the bottom) are: 2.34 Sv (0.58 Sv) net (southward), 6.4 Sv (1.48 Sv) in and 8.73 Sv (1.64 Sv) out of the Arctic Ocean. The net volume transport across the section H, east of Yermak Plateau is

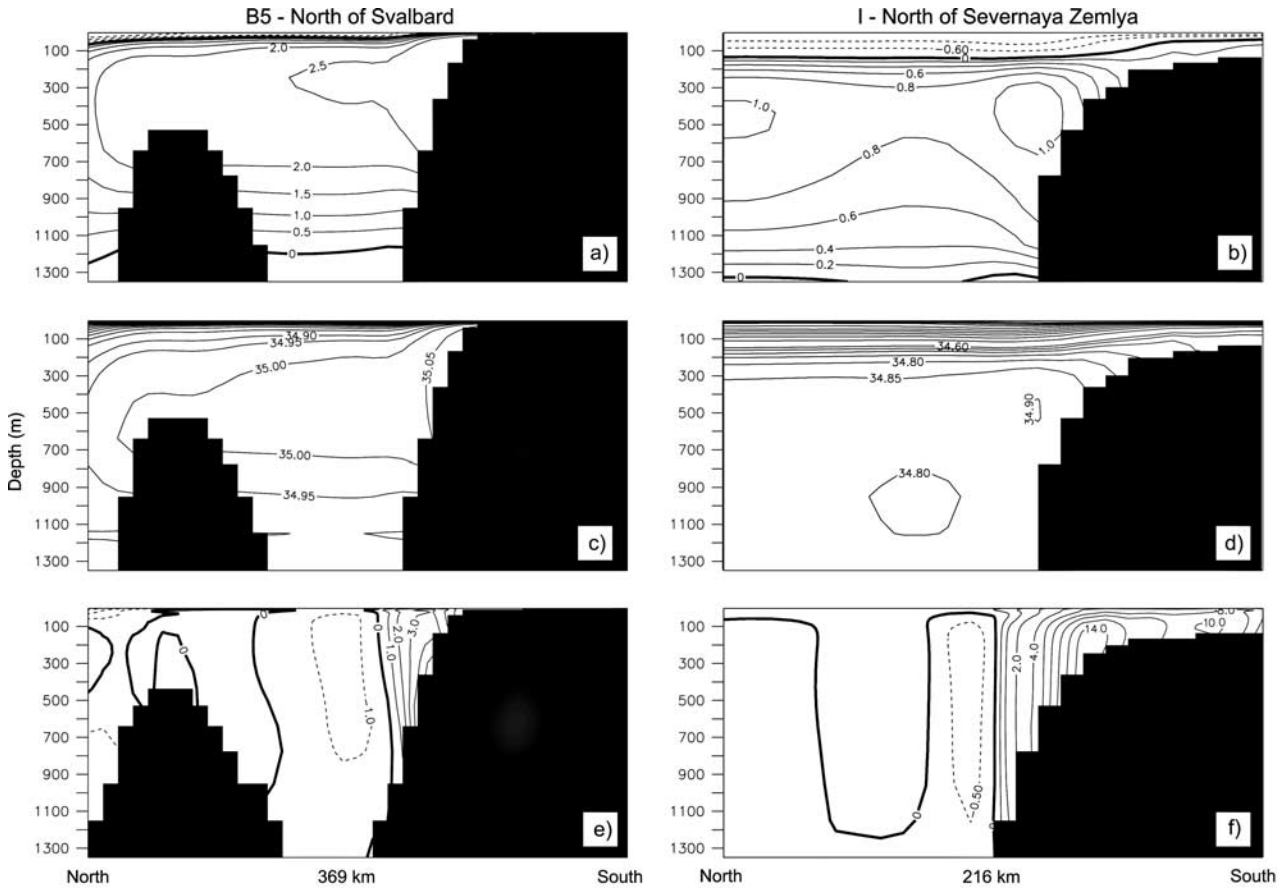

Figure 6. Vertical distribution of annual 23-year (a–b) mean potential temperature (°C), (c–d) salinity (psu), and (e–f) velocity (cm s^{-1}) across the section north of Svalbard (model section B5, left) and the section north of Severnaya Zemlya (model section I, right). Note the differing horizontal scales. Positive velocity contours represent eastward flows.

reduced to 1.55 Sv (0.82 Sv), suggesting that only about one quarter of the northward flowing West Spitsbergen Current passing the section B continues as the boundary current along the northern edge of the Barents Sea. The rest of this water recirculates further north within Fram Strait and/or enters the deep Nansen Basin. The net volume transport through the St. Anna and Voronin troughs is 2.61 Sv (2.32 Sv and 0.29 Sv, respectively), which is significantly larger (~70%) than that across section H, east of the Yermak Plateau. In summary, the Barents Sea branch of Atlantic water entering the Arctic Ocean contributes about 80% of water volume (of 3.19 Sv total net), 15% of heat flux (of 8.6 TW total net) and 82% of salt flux (of 110.4×10^3 kg s^{-1}), as measured at section I, north of Severnaya Zemlya. It is important to note that relative contributions to property fluxes are a function of the reference values (of temperature and salinity) used to calculate those fluxes.

[40] Previous modeling studies [e.g., *Holland et al.*, 1996; *Gerdes and Schauer*, 1997; *Zhang et al.*, 2000; *Karcher and Oberhuber*, 2002; *Karcher et al.*, 2003] have provided generally lower estimates of northward volume and property transports through Fram Strait. Direct comparison of flux estimates from those studies is difficult for many reasons, including different section locations, integration times, atmospheric forcing, lack of some calculations, etc. *Holland et al.* [1996], using a 1° isopycnal ice-ocean model of the Arctic and Atlantic Ocean with monthly climatological atmospheric forcing, report a 2.5 Sv net inflow into the Barents Sea and a 1.7 Sv net southward flow through Fram Strait (accompanied by a northward transport of about 1 Sv). *Gerdes and Schauer* [1997] use a similar domain, forcing, and resolution but with a *z*-level model, which yields a 3.2 Sv net southward flow through Fram Strait (with very weak northward transport) balanced by a 3.2 Sv net inflow into the Barents Sea. On the basis of their study, the net heat flux of 74 TW into the Barents Sea accounts for the total heat input into the Arctic Ocean and all fluxes significantly decrease when model vertical resolution is decreased. *Zhang et al.* [2000] estimate a net southward flux of 0.0–0.5 Sv, with 2.4–2.6 Sv to the north and 2.4–3.1 Sv to the south through Fram Strait and 0.9–1.4 Sv into the Barents Sea using a 40 km and 21-level ocean and sea ice model of the Arctic Ocean and subpolar seas forced with daily atmospheric data for 1979–1996. *Karcher and Oberhuber* [2002] using a similar resolution (i.e., 50 km grid) but isopycnal model forced with monthly mean ECMWF atmospheric climatological data for 1980–1989 obtain a net of 1.9 Sv

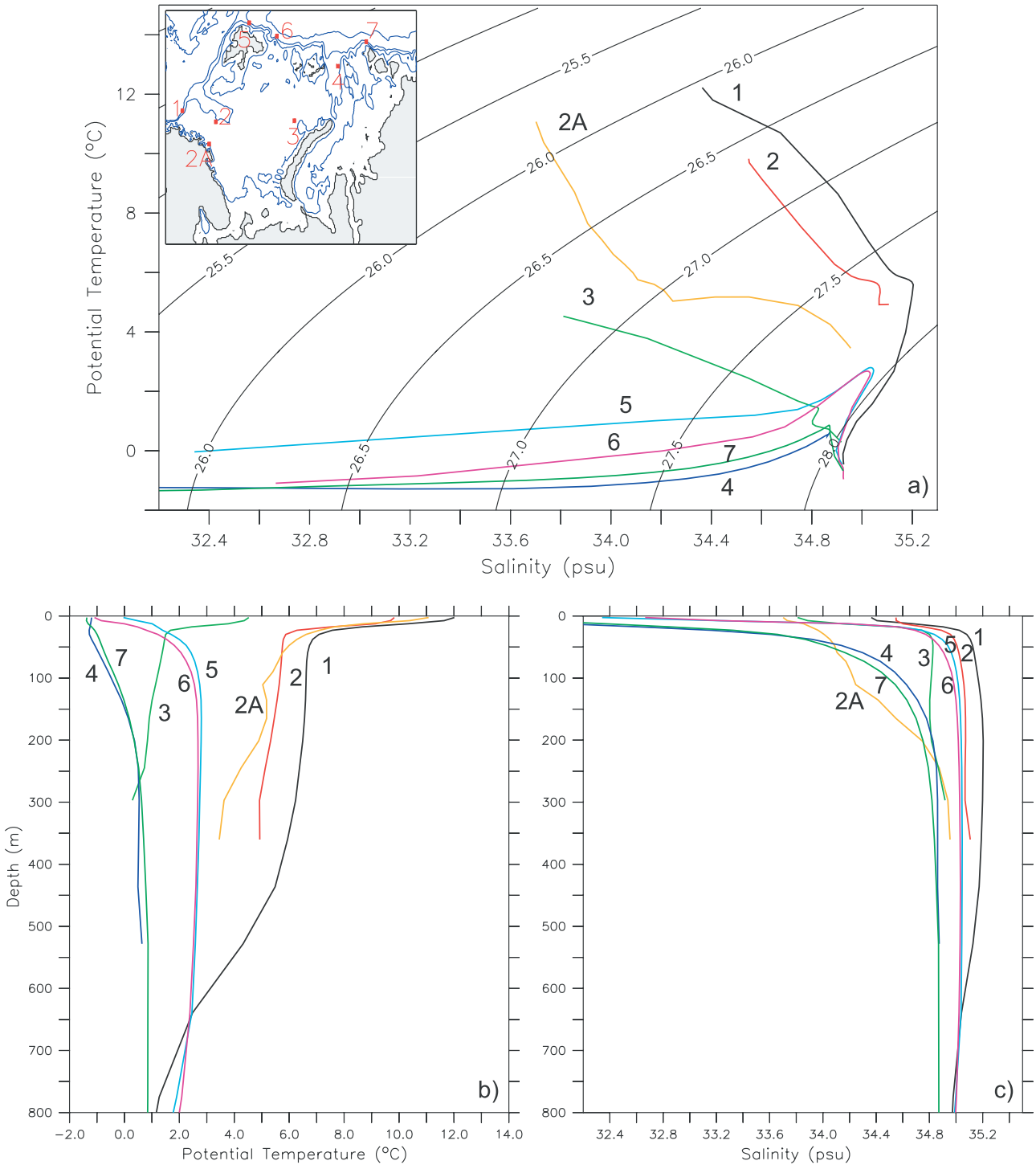

Figure 7. Summer average (July/August/September) (a) potential temperature (°C) versus salinity (psu), (b) vertical distribution of potential temperature (°C), and (c) vertical distribution of salinity (psu) for selected model stations in and around the Barents Sea. Each profile displayed represents an average over a 4 × 4 grid point region centered on the respective location shown in Figure 1.

southward (with 1.5 Sv in and 3.4 Sv out) through Fram Strait and a net of 2.3 Sv eastward (with 2.6 Sv in and 0.3 Sv out) into the Barents Sea.

[41] Our volume transports through Fram Strait are relatively higher compared to the above modeling studies, but they are still about 60–80% of those estimated from most recent high-density observations [*Fahrbach et al.*, 2001]. Earlier estimates of the West Spitsbergen Current transport based on relatively few current meters and 1- to 2-year-long time series range from 3 Sv [*Jonsson*, 1989], through 5.6 Sv [*Hanzlick*, 1983] and 7 Sv [*Greisman*, 1976], up to 8 Sv [*Aagaard et al.*, 1973]. Historical transports of the East

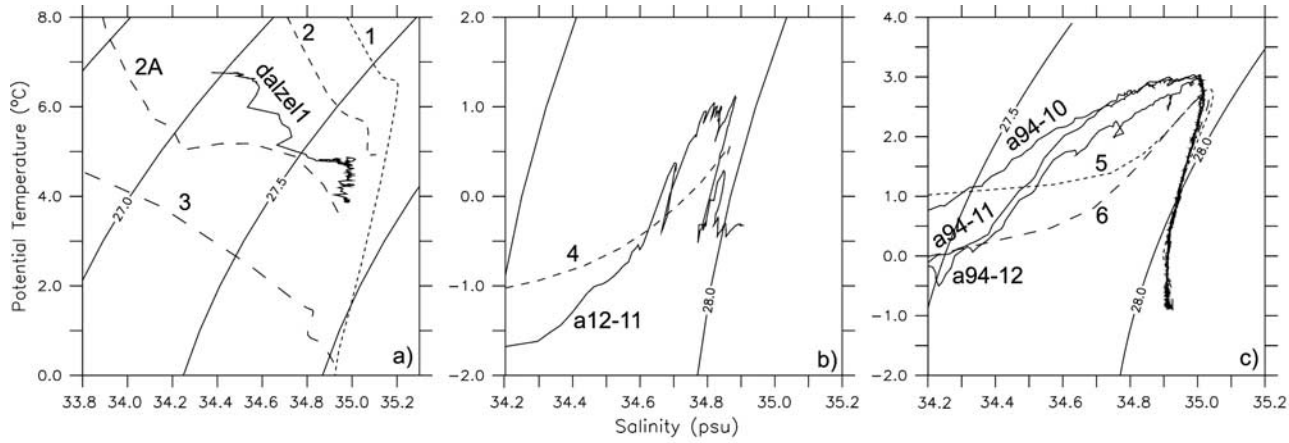

Figure 8. Potential temperature (°C) versus salinity (psu), modeled 23-year summer (July/August/September) mean and observations in the (a) western Barents Sea, in the (b) St. Anna Trough, and (c) north of Svalbard. Observational data include Dalnye Zelintsi 1 (July 1991) (dalzel1), *Polarstern* ARKXII (August/September 1996) (a12-11), and *Polarstern* ARKIX_4 (August/September 1993) (a94-10, 12). Note the differing temperature and salinity scales. See Figure 1 for station locations.

Greenland Current based on the total mass balance are from 2 Sv [*Mosby*, 1962], through 3.4 Sv [*Vowinckel and Orvig*, 1970] and 4.9 Sv [*Timofeyev*, 1962], to 7.1 Sv [*Aagaard and Greisman*, 1975]. *Foldvik et al.* [1988] report a southward flow of 3.0 Sv in the upper 700 m of the East Greenland Current based on current meter measurements. Similar arguments as to model-model comparisons apply to model-data and data-data comparisons, regarding differences in section locations, time of averaging, and spatial resolution/data coverage. Taking into account recirculation and eddies frequently present in the northern Greenland Sea, the most encouraging fact is that estimates of net transports through Fram Strait, i.e., a 1979–2001 mean of 2.34 Sv (std = 0.58 Sv) from the model compared to 4.2 Sv (std = 2.3 Sv) from 1997–1999 data [*Fahrbach et al.*, 2001], are within the range of uncertainties of both model and observational estimates. The lower flux estimates through Fram Strait from other models can be attributed in part to too weak (i.e., monthly mean) atmospheric forcing in some models or/and the model inability to realistically reproduce the full strength of opposite flowing boundary currents (i.e., the West Spitsbergen and East Greenland Current) and eddies within relatively narrow Fram Strait.

[42] The above discussion is provided to argue that the Barents Sea branch is an equally or possibly even more important source of mass, heat and salt to the central Arctic under the given atmospheric forcing. Model results are in support of earlier observations by *Rudels et al.* [1994] and the heat budget analysis by *Simonsen and Haugan* [1996]. Those studies suggest that the Barents Sea branch plays a crucial and equal role to the Fram Strait branch in the renewal of the intermediate and deep waters and the thermohaline circulation of the Arctic Ocean. It is yet to be determined the past and future changes in relative contributions of Barents Sea and Fram Strait branches under variable climate regimes, which in the region is dominated by the North Atlantic Oscillation (NAO). One could expect that during periods of strong positive North Atlantic Oscillation (NAO), when the predominant atmospheric forcing over the North Atlantic Ocean, the Norwegian Sea and the Barents Sea changes, increasing the frequency of storms reaching higher latitudes, and the inflow of Atlantic Water to the Barents Sea increases [*Dickson et al.*, 2000], the percent contribution of the Barents Sea branch of Atlantic Water to the boundary current along the shelf slope north of Severnaya Zemlya may increase significantly. At the same time the Fram Strait branch input may increase as well, so a question is how would the two inflows change relative to each other?

[43] Further validation of the model against data indicates that it realistically simulates the observed [*Schauer et al.*, 1997, 2002] northward displacement of the Fram Strait

Table 1. Model Sections and Stations[a]

Section	Name	Location
A	Svalbard-Norway	
A1	Norwegian Atlantic Current	
A2	Bear Island Trough	
B	Fram Strait	
B5	North of Svalbard	
C	Svalbard–Frans Josef Land	
D	Frans Josef Land–Novaya Zemlya	
E	St. Anna Trough	
F	Voronin Trough	
G	Severnaya Zemlya	
H	30°E	
I	95°E	
J	Kara Gate	
1	Norwegian Atlantic Current	71°36′N, 16°45′E
2	Bear Island Trough	73°36′N, 25°12′E
2A	Norwegian Coastal Current	71°00′N, 27°30′E
3	Novaya Zemlya Current	77°06′N, 52°18′E
4	St. Anna Trough	81°18′N, 73°12′E
5	North of Svalbard	80°54′N, 13°00′E
6	NE of Svalbard	82°09′N, 30°00′E
7	North of Severnaya Zemlya	82°18′N, 95°00′E

[a]Identified in Figure 1. Locations given for stations are the center point of a 36 km^2 (4 × 4 grid point) region. Profiles displayed for model stations are an average for that 36 km^2 region.

Table 2. Twenty-Three-Year Mean Volume Transport, Heat Transport (Qheat), and Total Salt Transport (Qsalt) Through Selected Sections[a]

		Volume			Qheat			Qsalt		
	Section Name	Net	Positive	Negative	Net	Positive	Negative	Net	Positive	Negative
A	Svalbard-Norway	3.27	5.07	−1.80	78.38	105.99	−27.61	114.15	177.17	−63.0
		0.58	**0.71**	**0.46**	**14.55**	**16.97**	**7.96**	**5.64**	**6.32**	**2.89**
A1	Norwegian Atlantic Current	7.70	9.52	−1.82	155.33	186.31	−30.98	270.19	333.94	−63.7
		2.31	**1.61**	**1.42**	**41.22**	**32.71**	**26.15**	**11.84**	**9.75**	**6.62**
A2	Bear Island Trough	3.23	5.91	−2.68	65.55	113.63	−48.08	112.88	206.64	−93.8
		0.57	**0.53**	**0.82**	**13.61**	**10.29**	**19.43**	**4.91**	**3.45**	**7.09**
B	Fram Strait	−2.34	6.40	−8.73	9.94	47.08	−37.15	−80.88	223.59	−304.
		0.58	**1.48**	**1.64**	**9.44**	**12.97**	**8.89**	**7.86**	**5.18**	**9.24**
B5	North of Svalbard	0.84	2.70	−1.86	12.90	23.60	−10.70	29.40	94.22	−64.8
		0.66	**0.67**	**0.40**	**7.69**	**7.69**	**3.18**	**2.79**	**2.26**	**2.55**
C	Svalbard–Frans Josef	−0.36	0.81	−1.17	0.76	2.37	−1.61	−12.55	28.23	−40.8
		0.20	**0.19**	**0.15**	**1.31**	**1.62**	**1.71**	**1.99**	**1.75**	**1.68**
D	Frans Josef–Novaya Zemlya	2.56	3.16	−0.61	2.15	2.58	−0.43	88.65	109.64	−21.0
		0.43	**0.47**	**0.08**	**3.45**	**3.68**	**0.44**	**6.43**	**6.92**	**1.52**
E	St. Anna Trough	2.32	2.92	−0.59	1.33	3.58	−2.24	80.38	101.04	−20.7
		0.39	**0.45**	**0.12**	**2.92**	**3.22**	**0.88**	**6.55**	**6.94**	**0.80**
F	Voronin Trough	0.29	0.72	−0.44	−0.28	0.04	−0.32	9.74	24.80	−15.1
		0.09	**0.15**	**0.08**	**0.49**	**0.70**	**0.55**	**2.33**	**2.75**	**1.23**
G	Severnaya Zemlya	0.31	0.32	−0.01	−0.96	−0.98	0.02	10.26	10.46	−0.20
		0.09	**0.09**	**0.002**	**0.32**	**0.32**	**0.008**	**7.48**	**7.44**	**0.25**
H	30°E	1.55	2.38	−0.83	10.74	14.23	−3.49	54.21	83.23	−29.0
		0.82	**0.73**	**0.38**	**6.43**	**6.26**	**2.03**	**1.50**	**1.47**	**0.72**
I	95°E	3.19	5.85	−2.66	8.58	13.59	−5.01	110.37	202.99	−92.6
		0.96	**1.10**	**1.01**	**4.07**	**3.93**	**1.93**	**7.88**	**8.69**	**4.01**
J	Kara Gate	0.32	0.33	−0.01	−0.70	−0.66	−0.04	10.64	10.91	−0.27
		0.13	**0.13**	**0.007**	**1.31**	**1.39**	**0.14**	**7.49**	**7.64**	**1.00**

[a]Positive and negative are defined as into and out of the Arctic Ocean, respectively, or following the path of Atlantic Water. Qheat is referenced to −0.1°C, and Qsalt is referenced to 0.0 psu. Calculations are for the entire water column, and standard deviations are shown in boldface. Volumes are in Sv, Qheat is in TW, and Qsalt is in 10^3 kg s^{-1}.

branch of Atlantic water inflow by the St. Anna Trough outflow (Figures 6a–6f). Temperature and salinity maxima are weakened and/or displaced off the continental slope by the Barents Sea branch inflow; and the area of eastward flow (positive velocity values) is broadened.

[44] In an effort to display the evolution of temperature and salinity along the flow of the two branches of Atlantic water through the Barents Sea and the Kara Sea in the model, eight stations were chosen representing entry, mid, and exit points (Figure 7). The station locations are based on the current distribution given by the 0–223 m July/August/September summer average current speed (spd = $\sqrt{u^2 + v^2}$, not shown). Across the major currents, the maxima of temperature and salinity were chosen for the station center (a luxury unique to analysis of high-resolution model output.) In order to better represent the significant water mass in that part of the flow, the profiles are averages over an area of $(36\ \text{km})^2$, a 4×4 grid point region.

[45] The temperature versus salinity diagrams and the vertical profiles (Figure 7) show warm, salty Atlantic Water entering the Barents Sea (stations 1, 2, 2A), which is cooled and freshened before it reaches the Eastern Basin (station 3) and which finally exits via the St. Anna Trough (station 4) after more cooling. Stations 1, 5, and 6 show the evolution of the Fram Strait branch of Atlantic Water as it enters the Arctic Ocean and is cooled and freshened as it travels east along the northern slope of the Barents Sea. The vertical distributions of temperature, salinity and velocity for these stations are visible in Figures 3a–3c and Figures 6a–6f. The colder, fresher St. Anna Trough outflow (station 4) combines with the Fram Strait branch (station 6) and the end result in temperature and salinity properties is shown at station 7.

[46] Model stations compare relatively well with selected observations (Figure 8, see Figure 1 and Table 1 for station locations) given the limitation of comparison of point measurements (in space and time) with model results (representing 1296 km^2 area and 23-year summer averages). Within these constraints, the agreement is good and thus we might be confident that the model simulates important characteristics of the water masses entering, transiting and exiting the Barents Sea reasonably well. The summer averaged model inflow into the Barents Sea is fresher at location 2A, which is much closer to the coast (and the fresh Norwegian Coastal Current) than the observed station d1. It is warmer and saltier than observations at location 2, which is set on the southern flank of Bear Island Trough in the warm and salty North Cape Current (Figure 8a). The coincidence of the modeled and observed temperature and salinity distribution in St. Anna Trough (Figure 8b) indicates appropriate cooling of the water in the model Barents Sea. Slight temperature departures there can again be explained by different locations of the observed station a12 and model station 4. A comparison of model station 3 with Norwegian observations taken west of Novaya Zemlya (courtesy of H. Loeng, not shown) suggests a reasonable rate of the cooling between model stations 2–2A and 3. The model captures the characteristics of the Fram Strait branch quite well when compared with observed data from August/September 1993 (Figure 8c). Owing to its larger cross section

(~50 km based on the velocity distribution in Figure 6c, the Fram Strait Branch is well represented in the model while small differences might suggest the need for inclusion of tides and eddies to improve mixing parameterizations.

[47] Since the high spatial resolution of the model allows analysis of eddies down to a scale of 36 km, we have investigated the distribution of eddy kinetic energy (EKE = $(u'^2 + v'^2)/2$) and its evolution with the increased model resolution. These calculations are done for daily fluctuations, referred to the annual mean. A daily snapshot represents the last time step out of the ~180 time steps during 1 day. Additionally, due to storage and integration time considerations, the daily snapshots contain velocity components among other limited variables at only a few depth levels. The annual mean velocity components, $\overline{u}$ and $\overline{v}$, were subtracted from the daily velocity values to obtain u' and v'. EKE was calculated for a region including the northern Norwegian, Greenland and Barents Seas. Annual mean surface EKE calculated from 1987 daily snapshots averaged 54.53 $cm^2\ s^{-2}$; with standard deviations about the mean of 70.2 $cm^2\ s^{-2}$. Comparison of EKE calculated in a similar region using output from an earlier, 18 km resolution model [*Maslowski et al.*, 2000] forced with the same atmospheric data, shows a 5 time increase in the area-averaged monthly mean EKE in the 9 km model over that in the 18 km model. Since the knowledge of time mean and eddy kinetic energy levels based on measurements is very limited, it is unclear what these values mean against the real ocean. At the same time models need to use such parameters to definitely quantify their level of realism in representing the region's dynamics and variability.

7. Summary

[48] Comparison of monthly averaged and daily snapshot model output with observations shows the high-resolution coupled ice-ocean model captures many of the important processes and water masses in the Barents Sea reasonably well. However, due in part to the small internal Rossby radius at high latitudes, some processes are not as well resolved.

[49] The free surface and high vertical resolution allow application of realistic bathymetry in the Barents Sea, which is the primary controlling factor of much of the circulation. As a result, the long-term circulation patterns agree well with earlier published maps [*Ozhigin et al.*, 2000]. The Atlantic Water flow through the Barents Sea, from the merging of portions of the North Cape Current and the Norwegian Coastal Current south of the Central Bank to the St Anna Trough outflow, is well defined. There is seasonal variability in the intensity of the flow, yet limited variability in the overall path. A comparison of model stations with selected observations suggest rather good agreement but indicates some space for improvements of subgrid-scale mixing processes parameterization. Mass and property transport magnitudes agree reasonably well with those calculated from observations. However, monthly and seasonal variability is smaller than some published observations. Under the prescribed atmospheric forcing, the mass, heat, and salt contributions of the Barents Sea branch of Atlantic Water to the central Arctic Ocean appear more or at least as significant as those of the Fram Strait branch. Calculations of EKE suggest seasonal variability as well as areas of increased activity apparently associated with local bathymetric features. The increase of model grid spacing, from 18 km and 30 levels to 9 km and 45 levels, has resulted in a 5 time increase in the mean EKE.

[50] **Acknowledgments.** A portion of this work is toward partial completion of the requirements for a Ph.D. in physical oceanography (D.M.). Funding for development and integration of the 9 km coupled ice-ocean model was provided by the ARCSS Program of the National Science Foundation, the Climate Change Prediction Program of the Department of Energy, and the Office of Naval Research. Computer resources were provided by the Arctic Region Supercomputer Center (ARSC), Fairbanks, Alaska, through the Department of Defense High Performance Computer Modernization Program (DOD/HPCMP) Grand Challenge project.

References

Aagaard, K. (1989), A synthesis of the Arctic Ocean circulation, *Rapp. P. V. Reun. Cons. Int. Explor. Mer.*, *188*, 11–22.

Aagaard, K., and P. Greisman (1975), Toward new mass and heat budgets for the Arctic Ocean, *J. Geophys. Res.*, *80*, 3821–3827.

Aagaard, K., C. Darnail, and P. Greisman (1973), Year-long current measurements in the Greenland-Spitsbergen passage, *Deep Sea Res. Oceanogr. Abstr.*, *20*, 743–746.

Antonov, J. I., S. Levitus, T. P. Boyer, M. E. Conkright, T. D. O'Brien, and C. Stephens (1998), *World Ocean Atlas 1998*, vol. 1, *Temperature of the Atlantic Ocean*, *NOAA Atlas NESDIS 27*, U.S. Govt. Print. Off., Washington, D. C.

Blindheim, J. (1989), Cascading of Barents Sea bottom water into the Norwegian Sea, *Rapp. P. V. Reun. Cons. Int. Explor. Mer.*, *188*, 49–58.

Boyer, T. P., S. Levitus, J. I. Antonov, M. E. Conkright, T. D. O'Brien, and C. Stephens (1998), *World Ocean Atlas 1998*, vol. 4, *Salinity of the Atlantic Ocean*, *NOAA Atlas NESDIS30*, U.S. Govt. Print. Off., Washington, D. C.

Dickson, R. R., T. J. Osborn, J. W. Hurrell, J. Meincke, J. Blindheim, B. Adlandsvik, T. Vinje, G. Alekseev, and W. Maslowski (2000), The Arctic Ocean response to the North Atlantic Oscillation, *J. Clim.*, *13*(15), 2671–2696.

Dukowicz, J. K., and R. D. Smith (1994), Implicit free-surface method for the Bryan-Cox-Semtner ocean model, *J. Geophys. Res.*, *99*, 7991–8014.

Environmental Working Group (1997), *Joint U.S.-Russian Atlas of the Arctic Ocean for the Winter Period* [CD-ROM], Natl. Snow and Ice Data Cent., Boulder, Colo.

Environmental Working Group (1998), *Joint U.S.-Russian Atlas of the Arctic Ocean for the Summer Period* [CD-ROM], Natl. Snow and Ice Data Cent., Boulder, Colo.

Fahrbach, E., J. Meincke, S. Osterhus, G. Rohardt, U. Schauer, V. Tverberg, and J. Verduin (2001), Direct measurements of volume transports through Fram Strait, *Pol. Res.*, *20*(2), 217–224.

Foldvik, A., K. Aagaard, and T. Torresen (1988), On the velocity field of the East Greenland Current, *Deep Sea Res., Part A*, *35*, 1335–1354.

Gerdes, R., and U. Schauer (1997), Large-scale circulation and water mass distribution in the Arctic Ocean from model results and observations, *J. Geophys. Res.*, *102*, 8467–8483.

Greisman, P. (1976), Current measurements in the eastern Greenland Sea, Ph.D. thesis, Univ. of Wash., Seattle.

Hanzlick, D. J. (1983), The West Spitsbergen Current: Transport, forcing, and variability, Ph.D. thesis, Univ. of Wash., Seattle.

Harms, I. H. (1997), Water mass transformation in the Barents Sea—Application of the Hamburg Shelf Ocean Model (HamSOM), *J. Mar. Sci.*, *54*, 351–365.

Harms, I. H., and M. J. Karcher (1999), Modeling the seasonal variability of hydrography and circulation in the Kara Sea, *J. Geophys. Res.*, *104*, 13,431–13,448.

Holland, D. M., L. A. Mysak, and J. M. Oberhuber (1996), An investigation of the general circulation of the Arctic Ocean using an isopycnal model, *Tellus, Ser. A*, *48*, 138–157.

Ingvaldsen, R., H. Loeng, and L. Asplin (2002), Variability in the Atlantic inflow to the Barents Sea based on a one-year time series from moored current meters, *Cont. Shelf Res.*, *22*(3), 505–519, doi:10.1016/S0278-4343(01)00070-X.

Jakobsson, M., N. Cherkis, J. Woodward, R. Macnab, and B. Coakley (2000), New grid of Arctic bathymetry aids scientists and mapmakers, *Eos Trans. AGU*, *81*(9), 89.

Johnson, D. R., T. A. McClimans, S. King, and O. Grennes (1997), Fresh water masses in the Kara Sea during summer, *J. Mar. Syst.*, *12*, 127–145.
Johnson, M. A., A. Y. Proshutinsky, and I. V. Polyakov (1999), Atmospheric patterns forcing two regimes of Arctic circulation: A return to anticyclonic conditions?, *Geophys. Res. Lett.*, *26*(11), 1621–1624.
Jonsson, S. (1989), The structure and forcing of the large- and mesoscale circulation in the Nordic Seas, with special reference to the Fram Strait, Ph.D. thesis, Univ. of Bergen, Norway.
Karcher, M. J., and J. M. Oberhuber (2002), Pathways and modification of the upper and intermediate waters of the Arctic Ocean, *J. Geophys. Res.*, *107*(C6), 3049, doi:10.1029/2000JC000530.
Karcher, M. J., R. Gerdes, F. Kauker, and C. Köberle (2003), Arctic warming: Evolution and spreading of the 1990s warm event in the Nordic seas and the Arctic Ocean, *J. Geophys. Res.*, *108*(C2), 3034, doi:10.1029/2001JC001265.
Killworth, P. D., D. Stainforth, D. J. Webb, and S. M. Patterson (1991), The development of a free surface Bryan-Cox-Semtner ocean model, *J. Phys. Oceanogr.*, *21*, 1333–1348.
Loeng, H. (1991), Features of the physical oceanographic conditions of the Barents Sea, *Pol. Res.*, *10*, 5–18.
Loeng, H., V. Ozhigin, B. Adlandsvik, and H. Sagen (1993), Current measurements in the northeastern Barents Sea, paper presented at the Statutory Meeting, Int. Counc. for the Explor. of the Sea, Dublin, Ireland.
Loeng, H., V. Ozhigin, and B. Adlandsvik (1997), Water fluxes through the Barents Sea, *ICES J. Mar. Sci.*, *54*, 310–317.
Maslowski, W., and W. Walczowski (2002), Circulation of the Baltic Sea and its connection to the pan-Arctic region—A large scale and high-resolution modeling approach, *Boreal Environ. Res.*, *7*(4), 319–325.
Maslowski, W., B. Newton, P. Schlosser, A. Semtner, and D. Martinson (2000), Modeling recent climate variability in the Arctic Ocean, *Geophys. Res. Lett.*, *27*(22), 3743–3746.
Maslowski, W., D. C. Marble, and W. Walczowski (2001), Recent trends in Arctic sea ice, *Ann. Glaciol.*, *33*, 545–550.
Matishov, G., A. Zyev, V. Golubev, N. Adrov, V. Slobodin, S. Levitus, and I. Smolyar (1998), *Climatic Atlas of the Barents Sea 1998: Temperature, Salinity and Oxygen*, *NOAA Atlas NESDIS 26*, U.S. Govt. Print. Off., Washington, D. C.
McClean, J., W. Maslowski, and M. Maltrud (2001), Towards a coupled environmental prediction system, *Lect. Notes Comput. Sci.*, *2073*, 1098–1107.
Mesinger, F., and A. Arakawa (1976), Numerical methods used in atmospheric models, paper presented at the Joint Organizing Comm., World Meteorol. Organ./Int. Counc. of Sci. Unions, Geneva, Switzerland.
Mosby, H. (1962), Water, salt, and heat balance of the North Polar Sea and of the Norwegian Sea, *Geophys. Publ.*, *24*, 289–313.
Nansen, F. (1906), Northern water: Captain Roald Amundsen's oceanographic observations in the Arctic Seas in 1901, *Videnskabs-Selskabets Skr., I, Math. Naturv.*, *1906*(3), 145 pp.
Ozhigin, V. K., A. G. Trofimov, and V. A. Ivshin (2000), The Eastern Basin Water and currents in the Barents Sea, paper presented at the Annual Science Conference, Int. Counc. for the Explor. of the Sea, Brugge, Belgium.
Parkinson, C. L., and W. M. Washington (1979), A large-scale numerical model of sea ice, *J. Geophys. Res.*, *84*, 311–337.
Parsons, A. R. (1995), On the Barents Sea Polar Front in summer and interpretations of the associated regional oceanography using an Arctic Ocean general circulation model, Ph.D. dissertation, Nav. Postgrad. Sch., Monterey, Calif.
Parsons, A. R., R. H. Bourke, R. D. Muench, C.-S. Chiu, J. F. Lynch, J. H. Miller, A. J. Plueddemann, and R. Pawlowicz (1996), The Barents Sea polar front in summer, *J. Geophys. Res.*, *101*, 14,201–14,221.
Pfirman, S. L., D. Bauch, and T. Gammelsrod (1994), The northern Barents Sea: Water mass distribution and modification, in *The Polar Oceans and Their Role in Shaping the Global Environment*, *Geophys. Monogr. Ser.* vol. 85, edited by O. M. Johannesen, R. D. Muench, and J. E. Overland, pp. 77–94, AGU, Washington, D. C.
Proshutinsky, A., and M. Johnson (1997), Two circulation regimes of the wind-driven Arctic Ocean, *J. Geophys. Res.*, *102*, 12,493–12,514.
Roach, A. T., K. Aagaard, C. H. Pease, S. A. Salo, T. J. Weingartner, V. Pavlov, and M. Kulakov (1995), Direct measurements of transport and water properties through the Bering Strait, *J. Geophys. Res.*, *100*, 18,443–18,457.
Rudels, B. (1987), On the mass balance of the Polar Ocean, with special emphasis on the Fram Strait, *Norw. Polarinst. Skr.*, *188*, 53 pp.
Rudels, B., and H. J. Friedrich (2000), The transformations of Atlantic Water in the Arctic Ocean and their significance for the freshwater budget, in *The Freshwater Budget of the Arctic Ocean*, edited by E. L. Lewis et al., pp. 503–532, Kluwer Acad., Norwell, Mass.
Rudels, B., E. P. Jones, L. G. Anderson, and G. Kattner (1994), On the intermediate depth waters of the Arctic Ocean, in *The Polar Oceans and Their Role in Shaping the Global Environment*, *Geophys. Monogr. Ser.* vol. 85, edited by O. M. Johannesen, R. D. Muench, and J. E. Overland, pp. 33–46, AGU, Washington, D. C.
Schauer, U., R. D. Muench, B. Rudels, and L. Timokhow (1997), Impact of eastern Arctic shelf waters on the Nansen Basin intermediate layers, *J. Geophys. Res.*, *102*, 3371–3382.
Schauer, U., B. Rudels, E. P. Jones, L. G. Anderson, R. D. Muench, G. Björk, J. H. Swift, V. Ivanov, and A.-M. Larsson (2002), Confluence and redistribution of Atlantic Water in the Nansen, Amundsen and Makarov basins, *Ann. Geophys.*, *20*(2), 257–273.
Semtner, A. J. (1976), A model for the thermodynamic growth of sea ice in numerical investigations of climate, *J. Phys. Oceanogr.*, *6*, 379–389.
Semtner, A. J. (1995), Modeling ocean circulation, *Science*, *269*, 1379–1385.
Semtner, A. J., Jr., and R. M. Chervin (1992), Ocean circulation from a global eddy-resolving model, *J. Geophys. Res.*, *97*, 5493–5550.
Simonsen, K., and P. M. Haugan (1996), Heat budgets of the Arctic Mediterranean and sea surface heat flux parameterizations for the Nordic Seas, *J. Geophys. Res.*, *101*, 6553–6576.
Steele, M., R. Morley, and W. Ermold (2000), PHC: A global ocean hydrography with a high quality Arctic Ocean, *J. Clim.*, *14*(9), 2079–2087.
Steele, M., W. Ermold, S. Häkkinen, D. Holland, G. Holloway, M. Karcher, F. Kauker, W. Maslowski, N. Steiner, and J. Zhang (2001), Adrift in the Beaufort Gyre: A model intercomparison, *Geophys. Res. Lett.*, *28*, 2935–2938.
Timofeyev, V. T. (1962), The movement of Atlantic water and heat into the Arctic Sea basin, *Deep Sea Res. Oceanogr. Abstr.*, *9*, 358–361.
Vowinckel, E., and S. Orvig (1970), The climate of the North Polar Basin, in *Climates of the Polar Regions*, edited by S. Orvig, pp. 129–226, Elsevier Sci., New York.
Zhang, J., D. A. Rothrock, and M. Steele (2000), Recent changes in Arctic sea ice: The interplay between ice dynamics and thermodynamics, *J. Clim.*, *13*, 3099–3114.
Zhang, Y., W. Maslowski, and A. J. Semtner (1999), Impact of mesoscale ocean currents on sea ice in high-resolution Arctic ice and ocean simulations, *J. Geophys. Res.*, *104*, 18,409–18,429.

J. L. Clement, W. Maslowski, and A. J. Semtner, Department of Oceanography, Naval Postgraduate School, 833 Dyer Road, Monterey, CA 93943, USA. (jlclemen@nps.navy.mil; maslowski@nps.navy.mil; sbert@ucar.edu)

D. Marble, Fleet Numerical Meteorology and Oceanography Center, U.S. Navy, Stop 1, 7 Grace Hopper Avenue, Monterey, CA 93943-5501, USA. (douglas.marble@fnmoc.navy.mil)

U. Schauer, Alfred Wegener Institute Foundation for Polar and Marine Research, Bussestrasse 24, D-27570, Bremerhaven, Germany. (uschauer@awi-bremerhaven.de)

W. Walczowski, Institute of Oceanology, Polish Academy of Sciences, ul. Powstánców Warszawy 55, PL-81-712, Sopot, Poland. (walczows@iopan.gda.pl)